A comparison of numerical methods for the large–scale modelling of acoustic coupled fluid-structure interactions of double-walled cylindrical shells

Herwig Peters[1]; Daniel Ryan Wilkes[2]

[1] School of Mechanical and Manufacturing Engineering, UNSW Australia, Sydney, NSW 2052, Australia.

[2] Centre for Marine Science and Technology, Curtin University, Perth, WA 6102, Australia.

ABSTRACT

This paper presents a comparison of numerical methods used to model large scale acoustic coupled fluid-structure interaction (FSI) problems for single and double-walled cylindrical shells. The finite element method (FEM) is used to model the structure while the fast multipole boundary element method (FMBEM) is used to model the fluid domain and both models are coupled on the shared boundary surface to allow for the FSI, yielding a coupled FEM-FMBEM formulation. At suitably high frequencies the statistical energy analysis (SEA) method may instead be used to model both the complete fluid domain and the structure. The FEM-FMBEM and SEA models are compared for two structural configurations. The first involves a single-walled cylindrical shell while the second case involves a double-walled cylindrical shell, where two cylindrical shells of different radii encapsulate an interior body of water. The SEA model is seen to provide substantially faster solution times at high frequencies, while yielding similar results to the FEM-FMBEM model.

Keywords: FEM, BEM, SEA, FMM, coupled fluid–structure interaction, double-walled cylindrical shell
I-INCE Classification of Subjects Number(s): 21.2.1, 75.2, 75.3, 75.5

1. INTRODUCTION

Underwater sound radiation from single and double-walled cylindrical shells may be numerically modelled as a coupled fluid–structure interaction (FSI) problem for which the acoustic and structural responses are solved simultaneously. Coupled FSI problems involving finite elastic structures submerged in unbounded fluid domains are typically modelled by coupling a finite element method (FEM) model of the interior elastic solid domain to a boundary element method (BEM) model of the exterior fluid domain via a coupling of the unknowns at the shared boundary surface between the two domains (1). Such a coupled FEM–BEM model configuration is advantageous as the FEM specifies material properties on a per–element basis, allowing for complex internal structures to be modelled, while the BEM represents the infinite exterior fluid domain by a surface–only discretisation.

The principal disadvantage of the coupled FEM–BEM models are due to the computational requirements of the BEM for large–scale problems, as the boundary surface must be discretised into a mesh with a certain number of boundary elements per fluid wavelength to achieve an acceptable solution accuracy (2). Thus, for large–scale problems the BEM discretisation yields a large number of elements/unknowns and the resulting coefficient matrix is fully populated and complex valued, being of size $N_{BE} \times N_{BE}$ for N_{BE} unknowns in the BEM domain. The direct solution of such a problem requires the order of $O(N_{BE}^3)$ operations, an iterative solution requires the order of $O(N_{BE}^2)$ operations per iteration, and the storage requirements of the matrix are proportional to $O(N_{BE}^2)$, all of which constitutes a prohibitive cost for large N_{BE}. The computational and memory requirements of the BEM may be substantially alleviated by applying the fast multipole method (FMM) (3) to the 3D Helmholtz boundary integral equation (BIE) used to represent the fluid domain (4). The fast multipole BEM (FMBEM) can reduce the algorithmic complexity of the matrix–vector products in the iterative BEM solution to $O(N_{BE}\log N_{BE})$ and the memory requirements to $O(N_{BE})$, depending on the frequency range of interest and FMM algorithm employed.

The use of coupled FEM–FMBEM formulations for large scale FSI problems was first implemented by Fischer and Gaul using a mortar coupling method between non–conforming meshes (5), and by Schneider

[1] herwig.peters@unsw.edu.au
[2] D.Wilkes@curtin.edu.au

using a direct coupling between conforming meshes (6). Such FEM–FMBEM models have been applied to a number of large scale models, including cylindrical shells (7), ship hulls (8, 9) and other partially submerged bodies (8, 10).

Higher frequency problems are better suited to probabilistic techniques, such as the statistical energy analysis (SEA) method (11), which can be similarly applied to coupled FSI problems (12, 13). SEA models represent the full problem as a series of simplified subsystems, where the storage, transport and dissipation of energy between subsystems provides the required coupling between subsystems to represent the full model. The main advantages of the SEA method are that the number of unknowns is not proportional to the problem wavelength (instead there is typically only one energy unknown per subsystem), and so the total problem size is significantly reduced compared to domain discretisation methods. The method also inherently provides statistical parameters of the model (mean, variance) without the need to run probabilistic simulations. The SEA model assumes that the subsystems are large compared to the wavelength of interest to allow for their statistical representation in the full model, and so the model is restricted to higher frequencies. In situations where an SEA subsystem is small compared to the wavelength in that domain, the response of the subsystem will be well defined by a small number of dominant mode shapes and so the statistical representation of the SEA will provide poor results. For these cases a hybrid FEM-SEA model may be employed, where the small subsystems are modelled with the FEM (14, 13).

In this paper, a coupled FSI problem for a cylindrical shell is treated via both an FEM–FMBEM model and an SEA model for two problem configurations. The first configuration involves a single-walled cylindrical shell with flat circular end plates submerged in water, and the second configuration involves a submerged double-walled cylindrical shell, where two cylindrical shells of different radii encapsulate an interior body of water and are similarly terminated by flat circular end plates. A comparison of the results using the two numerical approaches is presented for the two configurations. The paper is organised as follows. Section 2 provides details of the problem configurations for the two cylindrical shells, Section 3 briefly explains the formulation of the FEM, FMBEM and SEA models, Section 4 details the coupling formulations for the FSI and the corresponding numerical solution procedures for each model, Section 5 presents the numerical results for both single and double-walled cylindrical shells and discusses the relative performance of the different formulations used, and Section 6 presents the conclusions.

2. PROBLEM CONFIGURATIONS

This section provides details of the model configurations and material properties used for the single and double-walled cylindrical shells in the various numerical models. Schematics for the single and double-walled cylindrical shell configurations are presented in Figure 1 and the material properties of the water and steel are listed in Table 1.

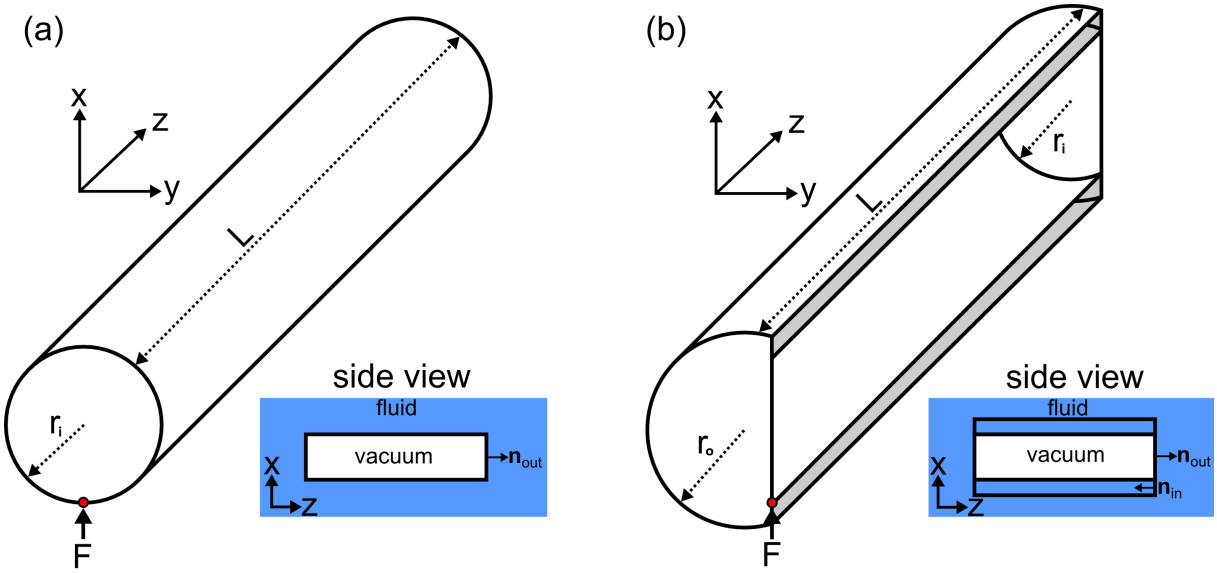

Figure 1 – Schematics for the single and double-walled cylindrical shells. The cross–sectional side view for each cylindrical shell (inset (a) and (b)) indicates the fluid domains and surface normals. Both models are excited by a point force F in the +x–direction applied at the junction of the small cylinder and one end plate.

Table 1 – Material properties for the single and double-walled cylindrical shells.

Parameter	Notation	Value	Unit
Density of water	ρ_f	1000	$\mathrm{kg/m^3}$
Sound speed in water	c_f	1500	$\mathrm{m/s}$
Density of steel	ρ_s	7860	$\mathrm{kg/m^3}$
Young's modulus (cylinder)	E_{cyl}	210	GPa
Young's modulus (end plates)	E_{end}	210	TPa
Poisson's ratio	ν	0.3	-

Note that the Young's modulus for the flat circular end plates has been artificially increased by three orders of magnitude (compared to the typical value for steel) to account for the fact that more realistic doubly-curved end closures such as hemispheres are much stiffer than the flat end plates used here, which otherwise would significantly affect the acoustic response of the cylinder models.

3. NUMERICAL MODELS

This section introduces the FEM, FMBEM and SEA methods used to model the coupled FSI formulations for both the single and double-walled cylindrical shells.

3.1 FEM

Assuming an $e^{-i\omega t}$ time dependence, the discretised FEM matrix equation for a finite structural domain takes the form (15)

$$\left(\mathbf{K} - i\omega\mathbf{D} - \omega^2\mathbf{M}\right)\mathbf{u} = \mathbf{f}_s \tag{1}$$

where $\mathbf{K}$, $\mathbf{D}$ and $\mathbf{M}$ are respectively the stiffness, damping and mass matrices, each being sparse, symmetric and of size $N_{FE} \times N_{FE}$ for N_{FE} structural unknowns, $\mathbf{u}$ and $\mathbf{f}_s$ are respectively the N_{FE} nodal vectors of the structural displacement unknowns and applied time–harmonic structural forces, $\omega = 2\pi f$ for frequency f and $i = \sqrt{-1}$. Here, the structural damping is modelled as frequency–independent hysteretic damping, and so the damping matrix $\mathbf{D}$ is related to the stiffness matrix $\mathbf{K}$ as

$$\mathbf{D} = (1 - i\eta)\,\mathbf{K} \tag{2}$$

where $\eta = 0.02$ applies a 2% structural loss factor. Here, the required FEM models are constructed in ANSYS using 8–node quadratic isoparametric shell elements and the resulting $\mathbf{K}$, $\mathbf{D}$ and $\mathbf{M}$ matrices are imported into the coupled FEM–FMBEM solver implemented in MATLAB.

3.2 FMBEM

The discretised Helmholtz boundary integral equation (BIE) for an exterior fluid domain using the Burton–Miller formulation (16) takes the form

$$\left(\alpha\frac{1}{2} + \mathbf{L} + \alpha\mathbf{L}'\right)\mathbf{q} - \left(-\frac{1}{2} + \mathbf{M} + \alpha\mathbf{M}'\right)\mathbf{p} = \mathbf{p}_i + \alpha\mathbf{q}_i \tag{3}$$

where $\mathbf{L}$, $\mathbf{L}'$, $\mathbf{M}$ and $\mathbf{M}'$ are the discretised coefficient matrices of the surface integrated Helmholtz Green's function and its normal surface derivatives, each being of size $N_{BE} \times N_{BE}$ for N_{BE} boundary unknowns, $\mathbf{p}$ and $\mathbf{q}$ are the N_{BE} nodal vectors of surface pressure and normal derivative of the surface pressure (related to the fluid particle velocity $\mathbf{v}_f = i\omega\rho_f\mathbf{q}$), $\mathbf{p}_i$ and $\mathbf{q}_i$ are the corresponding $\mathbf{p}/\mathbf{q}$ vectors for an incident acoustic field impinging the boundary surface and α is the Burton–Miller coupling parameter, chosen here to be $\alpha = \frac{0.05i}{k}$ for wavenumber k (17). Upon substitution of a suitable boundary condition to eliminate one of the surface unknowns ($\mathbf{p}$, $\mathbf{q}$), Equation (3) constitutes an exactly solvable system of equations for the N_{BE} unknowns.

The BEM coefficient matrices are fully populated, and so the computational/memory cost of the iterative BEM solution is proportional to $O(N_{BE}^2)$. The FMBEM reduces this algorithmic cost by approximately calculating the BEM matrix–vector product to a prescribed accuracy (17), but without explicitly forming nor directly multiplying the full coefficient matrix. The central idea of the FMBEM is to 'factorise' the fundamental solution of the Helmholtz BIE via series expansions, for example (17)

$$G(\mathbf{x},\mathbf{y}) = \frac{e^{ikr}}{4\pi r} = ik\sum_{n=0}^{\infty}\sum_{m=-n}^{n} S_n^m(\mathbf{x}-\mathbf{c})R_n^{-m}(\mathbf{y}-\mathbf{c}) \tag{4}$$

where $r = |\mathbf{x} - \mathbf{y}|$ for the source point $\mathbf{x}$ and receiver point $\mathbf{y}$. The S and R expansions may be independently calculated about a common expansion point $\mathbf{c}$ without requiring knowledge of *both* the source and receiver locations. This allows the FMBEM to apply interactions between groups of source and receiver points which share common expansion centres (Figure 2a), instead of explicitly calculating and storing the pairwise interactions between each pair of collocation points, as is done with standard BEM. Each local source group may only interact with the receiver groups which are 'well separated' from it, with the required separation distance being proportional to the geometric size of the group i.e. large groups may only interact over large separation distances. Thus, the FMM procedure is applied to the far field part of the surface integration for each receiver point, which can be envisaged as the large off–diagonal part of the full BEM coefficient matrix, while the sparse near field part of the BEM matrix (containing the regions of source points which are not well separated for each receiver) is directly calculated and stored (Figure 2b).

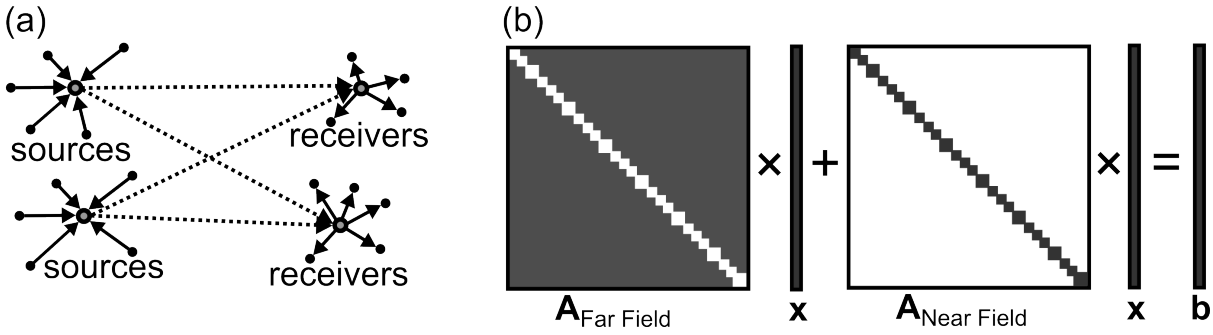

Figure 2 – Interactions between well separated groups of source/receiver points using multipole expansions with local expansion centres (a) and the corresponding equivalent calculation of the full BEM iterative solution matrix–vector products via the FMM (b). The large off-diagonal part of the coefficient matrix which represents the far field region of the surface integrals is treated by the FMM and so is not directly calculated/stored, while the sparse diagonal near–field region is calculated/stored as with the conventional BEM.

The required BEM models are constructed in GMSH using piecewise constant plane triangular elements with one collocation point in the centre of each element. These models are used in a broadband Helmholtz FMBEM (developed in MATLAB) which is coupled to the FEM for the FEM–FMBEM solver. The interested reader is referred to (17) for further details on broadband FMBEM models.

3.3 SEA

The SEA models the full structure as a series of interconnected subsystems whose average energies are related by the power injected into each subsystem and the power loss in each subsystem due to both dissipation within and coupling between subsystems. Applying a power balance for each subsystem yields a matrix equation of the form (12)

$$\mathbf{XE} = \mathbf{P} \tag{5}$$

where $\mathbf{X}$ is the coefficient matrix of subsystem dissipation and coupling loss factors of size $N_{SE} \times N_{SE}$ for N_{SE} statistical energy subsystems, $\mathbf{E}$ is the N_{SE}–element vector of average subsystem energies and $\mathbf{P}$ is the equal-sized vector of the input powers injected into each subsystem. For a set of coupled subsystems representing the full single and double-walled cylinders which have known dissipation/coupling loss factors and a known input power (i.e. due to the applied time–harmonic force), the subsystem energies $\mathbf{E}$ may be solved for and in turn used to calculate the radiated sound power from the cylinder models. The coupled FSI between the acoustic/structural domains and the incorporation of FE subsystems for the stiff end plates complicates the SEA implementation. The interested reader is referred to (12) and (13, 14) for details on the SEA for coupled FSI and the hybrid FEM-SEA models respectively. Here, the hybrid FEM-SEA models were constructed and solved using the VA One software suite developed by ESI.

4. COUPLING FORMULATIONS FOR FSI

This section presents the coupling formulations and solution methods employed to model the FSI between the fluid and solid domains, in particular for the FEM–FMBEM models of the single and double-walled cylinders. The analogous implementations for the hybrid FEM-SEA models are automatically applied by the VA One software between the corresponding FEM/SEA subsystems and hence are not discussed further.

The general coupling procedure for relating the unknowns between the FEM and FMBEM formulations applies the following continuity conditions at the shared boundary surface between the fluid/solid domains

1. The surface normal stress must be equal and opposite to the fluid pressure, while the tangential stress components must be zero as the fluid cannot support shear stresses (1). This condition is incorporated into the FEM matrix equation as an equivalent fluid loading force $\mathbf{f}_f$ via the coupling matrix $\mathbf{C}_{sf}$

$$\mathbf{f}_f = \mathbf{C}_{sf}\mathbf{p} \tag{6}$$

   which relates the FEM to the FMBEM unknowns on the structural surface and has rectangular dimensions of $N_{FE} \times N_{BE}$. Further details on the construction of coupling matrices is given by Peters et al. (18).
2. The required continuity of displacement normal to the shared boundary surface relates the FMBEM fluid particle velocities $\mathbf{v}_f$ to the FEM displacements as

$$\mathbf{v}_f = -i\omega\mathbf{C}_{fs}\mathbf{u} \tag{7}$$

   where $\mathbf{C}_{fs}$ is an analogous coupling matrix which relates the FMBEM to the FEM unknowns on the structural surface and has rectangular dimensions of $N_{BE} \times N_{FE}$ (18).

Thus, the coupled forms of Equations (1) and (3) which relate the displacements and pressures on the shared boundary surface can be written as a coupled matrix equation (assuming no incident acoustic field) as

$$\begin{bmatrix} \mathbf{K}_{FE} & -\mathbf{C}_{sf} \\ -i\omega\mathbf{G}\mathbf{C}_{fs} & \mathbf{H} \end{bmatrix} \begin{bmatrix} \mathbf{u} \\ \mathbf{p} \end{bmatrix} = \begin{bmatrix} \mathbf{f}_s \\ \mathbf{0} \end{bmatrix} \tag{8}$$

where

$$\mathbf{K}_{FE} = \left(\mathbf{K} - i\omega\mathbf{D} - \omega^2\mathbf{M}\right) \tag{9}$$

$$\mathbf{G} = \left(\alpha\frac{1}{2} + \mathbf{L} + \alpha\mathbf{L}'\right) i\omega\rho_f \tag{10}$$

$$\mathbf{H} = \left(\frac{1}{2} - \mathbf{M} - \alpha\mathbf{M}'\right) \tag{11}$$

The full coefficient matrix in Equation (8) is not explicitly constructed due to the FMBEM treatment of the $\mathbf{G}$ and $\mathbf{H}$ matrices. The following subsections present the iterative solution and preconditioning strategies used for the coupled FEM–FMBEM models based on Equation (8) for the single and double-walled cylindrical shells.

4.1 Single-Walled Cylindrical Shell FEM–FMBEM Solution

The coupled system of equations in Equation (8) representing the single-walled cylindrical shell may be directly solved using an iterative solution method such as the flexible GMRES (19) solver to simultaneously solve for both the structural displacements and surface pressures. However such methods are slow to converge (as shown by Brunner et al. (7)) and so the 'Schur complement' is used here to solve the reduced system

$$\left(\mathbf{H} - i\omega\mathbf{G}\mathbf{C}_{fs}\mathbf{K}_{FE}^{-1}\mathbf{C}_{sf}\right)\mathbf{p} = i\omega\mathbf{G}\mathbf{C}_{fs}\mathbf{K}_{FE}^{-1}\mathbf{f}_s \tag{12}$$

for pressure and the displacements are recovered from $\mathbf{p}$ as

$$\mathbf{u} = \mathbf{K}_{FE}^{-1}\left(\mathbf{f}_s + \mathbf{C}_{sf}\mathbf{p}\right) \tag{13}$$

The numerical solution of Equation (12) is advantageous as only the smaller set of N_{BE} pressure unknowns must be iteratively solved, but requires the inverse of the combined FEM matrix (Equation (9)) to be applied each iteration. In this work, the FEM matrix inverse is constructed using the Crout ILU factorisation with a zero drop tolerance, as well as reordering of $\mathbf{K}_{FE}$ using the symmetric approximate minimum degree permutation to reduce the fill–in of the resulting sparse lower/upper triangular matrices. The Crout implementation of the ILU typically reduces the storage requirements by a factor of 6 compared to the full LU matrices. The ILU matrices are thus precomputed and stored, and then called in each iteration of the solution, where the multiplication of $\mathbf{K}_{FE}^{-1}$ with the current solution vector via the ILU matrices is very fast to compute. Hence, the dominant cost in the iterative solution of Equation (12) is due to the FMBEM calculations of $\mathbf{G}$ and $\mathbf{H}$.

Equation (12) is solved using a flexible inner–outer iterative GMRES (fGMRES) solution method, where a fast low accuracy FMBEM is solved to a coarse convergence tolerance of 0.2 in the inner GMRES loop, and this preconditioned solution is then used in the full accuracy FMBEM in the outer GMRES loop, which is solved to a fine convergence tolerance of 10^{-5}. In both cases the required $\mathbf{K}_{FE}^{-1}$ multiplication operations are calculated using the same ILU matrices. Additionally, the inner GMRES loop is itself preconditioned using a sparse approximate inverse (SAI) preconditioner (20) constructed from the sparse near field FMBEM matrices.

4.2 Double-Walled Cylindrical Shell FEM–FMBEM Solution

The double-walled cylindrical shell involves both an infinite exterior fluid domain coupled to the outer shell and the finite interior fluid region encapsulated by the outer and inner shells, with both regions treated here using the FMBEM. The governing Helmholtz BIE for the interior fluid domain has exactly the same form as in Equation (3) for the infinite exterior domain. The surface normal is defined as pointing towards the interior fluid as indicated by $\mathbf{n}_{\text{in}}$ in the inset of Figure 1b. The exterior and interior FMBEM models must then be independently coupled to the structural FEM via separate coupling matrices which relate the structural unknowns on the outer/inner FEM surface to the corresponding FMBEM models. Denoting the exterior and interior FMBEM pressure unknowns as $\mathbf{p}^{\text{ext}}$ and $\mathbf{p}^{\text{int}}$ respectively thus yields the following matrix equation

$$\begin{bmatrix} \mathbf{K}_{FE} & -\mathbf{C}_{sf}^{\text{ext}} & -\mathbf{C}_{sf}^{\text{int}} \\ -i\omega\mathbf{G}^{\text{ext}}\mathbf{C}_{fs}^{\text{ext}} & \mathbf{H}^{\text{ext}} & \mathbf{0} \\ -i\omega\mathbf{G}^{\text{int}}\mathbf{C}_{fs}^{\text{int}} & \mathbf{0} & \mathbf{H}^{\text{int}} \end{bmatrix} \begin{bmatrix} \mathbf{u} \\ \mathbf{p}^{\text{ext}} \\ \mathbf{p}^{\text{int}} \end{bmatrix} = \begin{bmatrix} \mathbf{f}_s \\ \mathbf{0} \\ \mathbf{0} \end{bmatrix} \tag{14}$$

where $\mathbf{C}_{sf}^{\text{ext}}$ and $\mathbf{C}_{sf}^{\text{int}}$ are the FEM to FMBEM coupling matrices for the exterior and interior FMBEM vectors of pressure unknowns respectively, $\mathbf{C}_{fs}^{\text{ext}}$ and $\mathbf{C}_{fs}^{\text{int}}$ are the corresponding FMBEM to FEM coupling matrices, and the $\mathbf{H}$ and $\mathbf{G}$ matrices for the exterior/interior fluid domains are similarly denoted by the $^{\text{ext}}$ and $^{\text{int}}$ superscripts. In particular it should be noted that there is no explicit coupling between the exterior and interior pressures in Equation (14), as indicated by the all–zero submatrices in the coupled coefficient matrix, and so the only interaction between the exterior and interior fluid domains is through the coupling to the structural FEM. The Schur complement for Equation (14) simultaneously solves for both the exterior and interior pressures

$$\left(\begin{bmatrix} \mathbf{H}^{\text{ext}} & \mathbf{0} \\ \mathbf{0} & \mathbf{H}^{\text{int}} \end{bmatrix} - i\omega \begin{bmatrix} \mathbf{G}^{\text{ext}} & \mathbf{0} \\ \mathbf{0} & \mathbf{G}^{\text{int}} \end{bmatrix} \begin{bmatrix} \mathbf{C}_{fs}^{\text{ext}} \\ \mathbf{C}_{fs}^{\text{int}} \end{bmatrix} \mathbf{K}_{FE}^{-1} \begin{bmatrix} \mathbf{C}_{sf}^{\text{ext}} & \mathbf{C}_{sf}^{\text{int}} \end{bmatrix} \right) \begin{bmatrix} \mathbf{p}^{\text{ext}} \\ \mathbf{p}^{\text{int}} \end{bmatrix} = i\omega \begin{bmatrix} \mathbf{G}^{\text{ext}} & \mathbf{0} \\ \mathbf{0} & \mathbf{G}^{\text{int}} \end{bmatrix} \begin{bmatrix} \mathbf{C}_{fs}^{\text{ext}} \\ \mathbf{C}_{fs}^{\text{int}} \end{bmatrix} \mathbf{K}_{FE}^{-1} \mathbf{f}_s \tag{15}$$

and the displacements may then be recovered as

$$\mathbf{u} = \mathbf{K}_{FE}^{-1} \left(\mathbf{f}_s + \begin{bmatrix} \mathbf{C}_{sf}^{\text{ext}} & \mathbf{C}_{sf}^{\text{int}} \end{bmatrix} \begin{bmatrix} \mathbf{p}^{\text{ext}} \\ \mathbf{p}^{\text{int}} \end{bmatrix} \right) \tag{16}$$

Equation (15) is similarly solved using a flexible inner–outer iterative GMRES solution method (using the same convergence tolerances as previously specified), $\mathbf{K}_{FE}^{-1}$ is applied using the ILU factorisation and the fast low accuracy FMBEM for the inner GMRES loop is now preconditioned using a block diagonal form of the SAI preconditioners (applied separately to the exterior/interior FMBEM models).

5. NUMERICAL RESULTS

Numerical results for the single and double-walled cylindrical shells are presented from both the FEM–FMBEM and FEM–SEA models in the form of the radiated sound power and the far field pressure. FEM–FMBEM pressure/displacement results are also shown for each of the highest modelled frequencies. All FEM–FMBEM models were solved on the Leonardi High Performance Computing cluster at the Faculty of Engineering, UNSW Australia, requiring one 64 processor node with 120GB of RAM for the largest models. The FEM–SEA models were solved on a standard desktop workstation.

5.1 Single-Walled Cylindrical Shell

Figure 3 shows the real components of the pressure and displacement for the FEM–FMBEM single-walled cylindrical shell at the highest modelled frequency of 700Hz. The pressure range in Pascals is indicated by the colour bar (Figure 3a), while the FEM displacement field in Figure 3b has been greatly exaggerated using a scaling factor to show the surface variation (red wire frame mesh) compared to the unperturbed mesh (green wire frame mesh). The outward radial displacements correspond to positive pressures on the cylindrical shell as expected, while the dominant surface variation in the results corresponds to a flexural wave which has a smaller wavelength than both the shear wavelength in the steel and compressional wavelength in the fluid.

Figure 4 presents the total radiated sound power and far field pressure versus frequency for the single-walled cylindrical shell calculated using both the FEM–FMBEM and FEM–SEA methods. The FEM–FMBEM

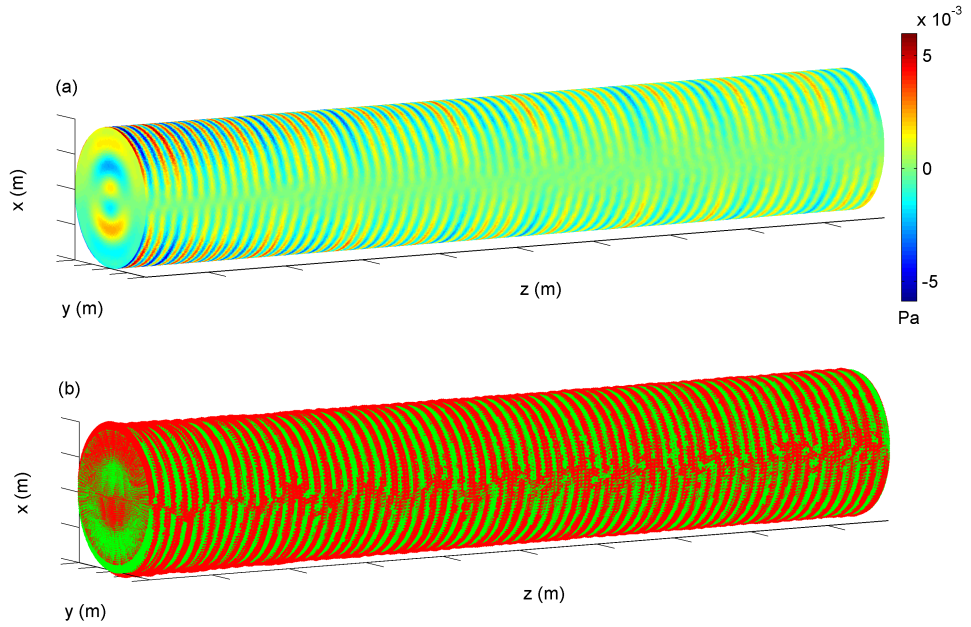

Figure 3 – Real components of the coupled pressure and displacement results from the FEM–FMBEM single-walled cylindrical shell at 700Hz. At this frequency the FEM mesh consists of 30,720 quadratic isoparametric shell elements and the FMBEM mesh consists of 132,102 piecewise constant plane triangular elements.

results are presented for three mesh discretisations used over the different frequency ranges as indicated in Figure 4. Good agreement is observed between the overlapping frequency regions between the successively refined FEM–FMBEM meshes. Below 80Hz a number of peaks are observed in the FEM–FMBEM results which correspond to the low order cylinder bending modes excited by the applied transverse point force. The FEM–SEA model is unable to provide reliable results at the lower frequencies due to both the low modal density over this frequency range and the inherent averaging effect of the method. Reasonable agreement between the FEM–SEA and FEM–FMBEM models is observed above 150Hz, where both models predict a peak in the radiated sound power between 150–200Hz corresponding to the cylinder ring frequency of the single-walled cylindrical shell, followed by a slow decay with increasing frequency. The FEM–SEA model is seen to consistently overpredict the radiated sound power compared to the FEM–FMBEM model above 200Hz.

5.2 Double-Walled Cylindrical Shell

Figure 5 shows the real components of the pressure and displacement for the FEM–FMBEM double-walled cylindrical shell on the exterior shell surface, while Figure 6 shows similar results for the interior fluid region and the inner shell surface. For both figures the pressure ranges are indicated by the respective colour bars, while the displacements have again been exaggerated using a common scaling factor to show the surface variation (red wire frame meshes) compared to the unperturbed mesh (green wire frame meshes). The outer and inner cylindrical shells can be seen to be vibrating in phase, while the positive radial displacements of the outer cylindrical shell correspond to positive pressures on the outer shell surface and negative pressures on the outer surface of the inner fluid domain (i.e. on the underside of the outer cylindrical shell). Again, the dominant surface variation in the double-walled cylindrical shell pressures and displacements correspond to a flexural wave whose wavelength is much smaller than that of the shear and compressional waves in the solid and fluid media, respectively.

Figure 7 presents the total radiated sound power and far field pressure versus frequency for the double-walled cylindrical shell calculated using both the FEM–FMBEM and SEA methods. The FEM–FMBEM results are presented for two mesh discretisations used over the different frequency ranges. Discrepancies between the calculated sound power/far field pressure results between the two mesh discretisations can be seen above 125Hz, indicating that the coarser mesh does not have an adequate mesh resolution to solve the problem above this frequency. Good agreement is observed in the overlapping 100–125Hz range for the two meshes. The FEM–FMBEM model similarly predicts a number of cylinder bending modes below 80Hz which are again absent in the FEM–SEA results, as was the case for the single-walled cylindrical shell. Reasonable agreement between the FEM–SEA and FEM–FMBEM models is observed above 125Hz, where both models predict a

peak in the radiated sound power at approximately 150Hz corresponding to the cylinder ring frequency of the double-walled cylindrical shell, followed by a slow decay with increasing frequency.

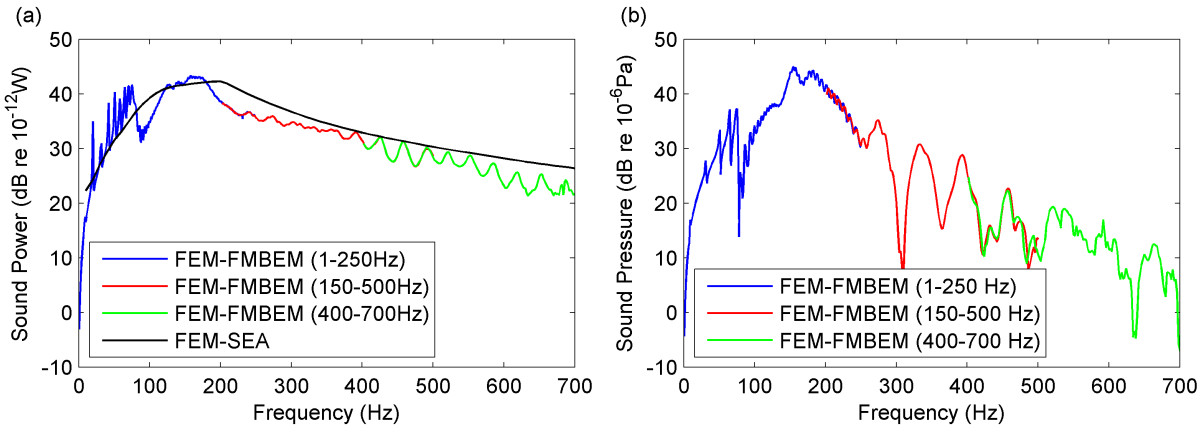

Figure 4 – Total radiated sound power (a) and far field pressure (b) versus frequency for the single-walled cylindrical shell.

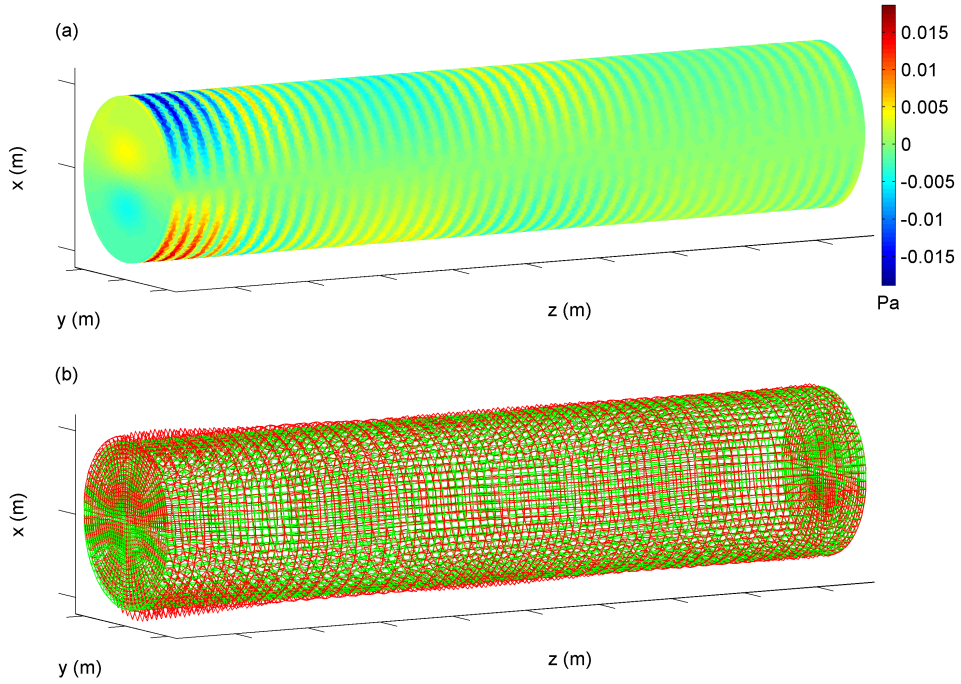

Figure 5 – Real components of the coupled pressure and displacement results from the FEM–FMBEM double-walled cylindrical shell at 200Hz for the outer shell surface. At this frequency the FEM mesh consists of 14,336 quadratic isoparametric shell elements and the outer FMBEM mesh consists of 42,596 piecewise constant plane triangular elements.

6. CONCLUSIONS

This paper has presented a comparison of the numerical results for the FEM–FMBEM and SEA models for two large scale models involving a single and a double-walled cylindrical shell. Good agreement between the deterministic and statistic models was observed at frequencies above 150Hz for the single-walled cylindrical shell and 125Hz for the double-walled cylindrical shell, while the FEM–SEA model was several orders of magnitude faster and required very minimal computational resources and is recommended to be used above these frequencies. At frequencies below 125–150Hz, or at any frequency where the full coupled displacement and pressure fields are required, the FEM–FMBEM model is recommended.

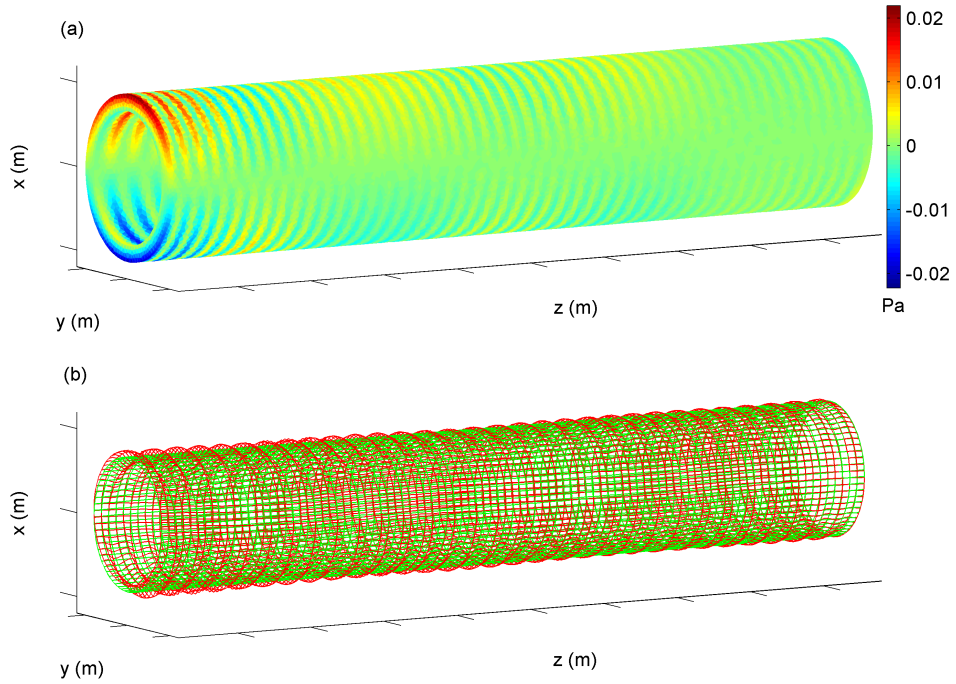

Figure 6 – Real components of the coupled pressure and displacement results from the FEM–FMBEM double-walled cylindrical shell at 200Hz for the inner cylindrical shell surface. At this frequency the FEM mesh consists of 14,336 quadratic isoparametric shell elements and the inner FMBEM mesh consists of 69,440 piecewise constant plane triangular elements.

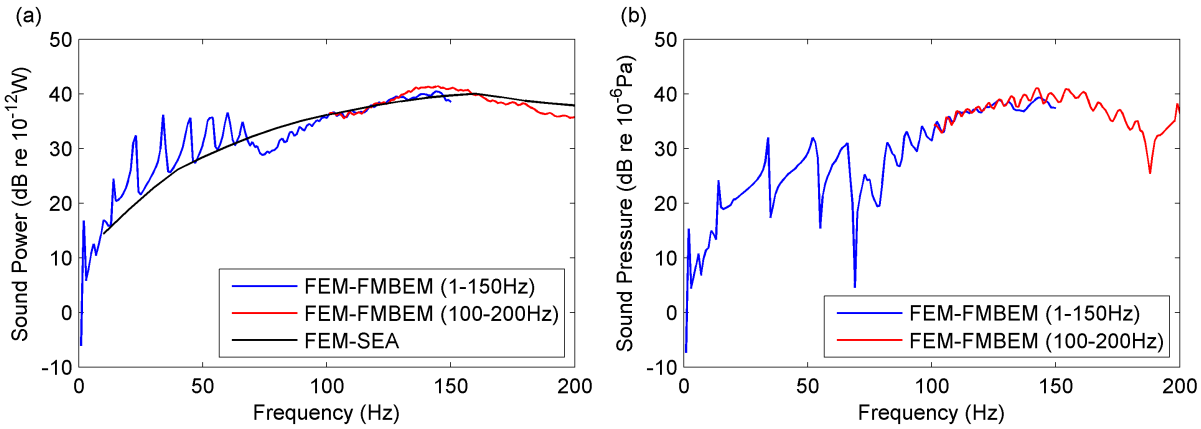

Figure 7 – Total radiated sound power (a) and far field pressure (b) versus frequency for the double-walled cylindrical shell.

7. ACKNOWLEDGEMENTS

Compute time on the Leonardi High Performance Computing cluster at the Faculty of Engineering, UNSW Australia, is gratefully acknowledged. The second author would like to thank A/Prof. Nicole Kessissoglou (UNSW Australia) for funding support.

REFERENCES

1. Amini S, Harris PJ, Wilton DT. Coupled Boundary and Finite Element Methods for the Solution of the Dynamic Fluid-Structure Interaction Problem. Brebbia CA, Orszag SA, editors. no. 77 in Lecture Notes in Engineering. Berlin: Springer-Verlag; 1992.

2. Marburg S. Six boundary elements per wavelength: Is that enough? J Comput Acoust. 2002;10(1):25–51.

3. Greengard L, Rokhlin V. A fast algorithm for particle simulations. J Comput Phys. 1987;73:325–348.

4. Coifman R, Rockhlin V, Wandzura S. The fast multipole method for the wave equation: A pedestrian prescription. IEEE Antennas Propagat Mag. 1993;35:7–12.

5. Fischer M, Gaul L. Fast BEM-FEM mortar coupling for acoustic-structure interaction. Int J Numer Meth Eng. 2005;62:1677–1690.

6. Schneider S. FE/FMBE coupling to model fluid-structure interactions. Int J Numer Meth Eng. 2008;76:2137–2156.

7. Brunner D, Junge M, Gaul L. A comparison of FE-BE coupling schemes for large-scale problems with fluid-structure interaction. Int J Numer Meth Eng. 2009;77:664–688.

8. Brunner D, Junge M, Cabos C, Gaul L. Vibroacoustic simulation of partly immersed bodies by a coupled fast BE-FE approach. In: Proceedings of Acoustics '08. Paris, France; 2008. .

9. Junge M, Brunner D, Gaul L. Solution of FE-BE coupled eigenvalue problems for the prediction of the vibro-acoustic behaviour of ship-like structures. Int J Numer Meth Eng. 2011;87:664–676.

10. Brunner D, Of G, Junge M, Steinbach O, Gaul L. A fast BE-FE coupling scheme for partly immersed bodies. Int J Numer Meth Eng. 2010;81:28–47.

11. Fahy FJ. Statistical Energy Analysis: A Critical Overview. Phil Trans R Soc A. 1994;346:431–447.

12. Liu M, Keane AJ, Taylor RE. Modelling liquid-structure interactions within the framework of statistical energy analysis. J Sound Vib. 2000;238(4):547–574.

13. Langley RS, Cordioli JA. Hybrid deterministic-statistical analysis of virbo-acoustic systems with domain couplings on statistical components. J Sound Vib. 2009;321:893–912.

14. Cotoni V, Shorter P, Langley R. Numerical and experimental validation of a hybrid finite element-statistical energy analysis method. J Acoust Soc Am. 2007;122(1):259–270.

15. Zienkiewicz OC, Taylor RL. Finite Element Method. vol. 1. 5th ed. Elsevier; 2000.

16. Burton AJ, Miller GF. The application of integral equation methods to the numerical solution of some exterior boundary value problems. Proc R Soc A. 1971;323(1553):201–210.

17. Gumerov NA, Duraiswami R. A broadband fast multipole accelerated boundary element method for the 3D Helmholtz equation. J Acoust Soc Am. 2009 January;125(1):191–205.

18. Peters H, Marburg S, Kessissoglou N. Structural-acoustic coupling on non-conforming meshes with quadratic shape functions. Int J Numer Meth Eng. 2012;91:27–38.

19. Saad Y. A flexible inner-outer preconditioned GMRES algorithm. SIAM J Sci Comput. 1993;14:461–469.

20. Chen K, Harris PJ. Efficient preconditioners for iterative solution of the boundary element equations for the three-dimensional Helmholtz equation. Appl Numer Math. 2001;36:475–489.